

Article

Evolution of Structure and Properties of Micro-Nano Structure 2507 Duplex Stainless Steel Prepared by Aluminothermic Reduction

Faqi Zhan ¹, Xiao Liu ², Hua Zhang ², Keliang Wang ², Shipeng Xu ³, Min Zhu ^{2,*}, Yuehong Zheng ¹ and Peiqing La ^{1,*}

- ¹ State Key Laboratory of Advanced Processing and Recycling of Nonferrous Metals, Lanzhou University of Technology, Lanzhou 730050, China; zhanfaqi@lut.edu.cn (F.Z.); zhengyuehong1986@126.com (Y.Z.)
² School of Materials Science and Engineering, Lanzhou University of Technology, Lanzhou 730050, China; lxiao0204@163.com (X.L.); zh418603@163.com (H.Z.); w1761818577@163.com (K.W.)
³ Gansu Key Laboratory of Solar Power Generation System Project, Jiuquan Vocational and Technical College, Jiuquan 735000, China; shipeng4425660@126.com
* Correspondence: zhumin@lut.edu.cn (M.Z.); pqla@lut.cn (P.L.)

Abstract: In this work, a large ingot of micro-nano structure 2507 duplex stainless steel was prepared in a single step using the aluminothermic reaction method. Chromium having different excess fractions were added to reaction powders to make up for evaporation loss, and the results show that the composition and structure of 2507 duplex stainless steel with a chromium excess ratio of 70% are satisfactory. The volume fraction of nanocrystalline in as-cast alloy was 41% and the average grain size was 34 nm. Additionally, the anticipated steels were rolled roughly with deformation of 40% at 1000 °C and followed by fine rolling with deformation of 30, 50 and 70%, separately, at 800 °C. Then, the effects of rolling deformation and precipitation on mechanical properties were studied in detail. Compared with the as-cast alloy, there was no phase transformation in the alloys with deformation of 30 and 50%, and they were still composed of γ and α phases, whereas the σ phase appeared in the alloy with deformation of 70%. When the deformation was 50%, the rolled alloy achieved the best performance, and the tensile strength, yield strength, and elongation were 912 MPa, 523 MPa, and 24.3%, respectively.

Keywords: micro-nano structure; 2507 duplex stainless steel; rolling deformation; mechanical property; aluminothermic reaction



Citation: Zhan, F.; Liu, X.; Zhang, H.; Wang, K.; Xu, S.; Zhu, M.; Zheng, Y.; La, P. Evolution of Structure and Properties of Micro-Nano Structure 2507 Duplex Stainless Steel Prepared by Aluminothermic Reduction. *Crystals* **2022**, *12*, 848. <https://doi.org/10.3390/cryst12060848>

Academic Editors: Marina Polyakova, Marina Samodurova and Cyril Cayron

Received: 15 May 2022

Accepted: 10 June 2022

Published: 16 June 2022

Publisher's Note: MDPI stays neutral with regard to jurisdictional claims in published maps and institutional affiliations.



Copyright: © 2022 by the authors. Licensee MDPI, Basel, Switzerland. This article is an open access article distributed under the terms and conditions of the Creative Commons Attribution (CC BY) license (<https://creativecommons.org/licenses/by/4.0/>).

1. Introduction

The 2507 duplex stainless steel is composed of ferrite (α) and austenite (γ) phases [1,2], and has high strength resulting from the ability of the α phase to resist chloride stress corrosion, in addition to the excellent plasticity and welding properties of the γ phase. Therefore, it is widely used in marine engineering, petrochemical, food, medical equipment, nuclear power, and other fields [3–5]. The current research of 2507 duplex stainless steel mainly focuses on improving its corrosion resistance and strength by alloying methods [6–9]; for instance, the chromium, molybdenum, nitrogen, and manganese alloying elements can not only improve the strength, hardness, and recrystallization temperature, but also obtain excellent pitting corrosion resistance, chloride ion corrosion resistance, and uniform corrosion resistance to acid due to the improvement in the stability of the passive film [10–13]. Moreover, the rare earth element cerium can improve the as-cast structure of steel and increase its plasticity and impact toughness. In addition to the alloying method, the hardness of 2507 duplex stainless steel can be significantly improved by increasing the precipitation amount of various phases (σ phase, τ phase, χ phase) by increasing the aging time [14–16]. However, these phases are hard and brittle intermetallic compound phases that significantly deteriorates the mechanical and corrosion-resistant properties of duplex

stainless steel. Prokofiev, et al. developed a non-destructive test of the σ phase by magnetic saturation polarization and thermoelectric power measurements [17]. Berecz, et al. studied the effects of cold working on the phase transformations of duplex stainless steels and these transformations were identified as the formation of α' - and σ -phases [18]. It is known that a medium work hardening layer can be obtained with high residual compressive stress using the multiple shot peening treatment, which improves the surface quality, fatigue life, and wear resistance of the alloy [19]. Undoubtedly, the properties of steels can be improved by either alloying or special processing; however, these two methods also introduce challenges relating to composition control, the complex process, and cost.

In recent years, researchers have found that the grain size and micro-nano crystalline ratio can be adjusted to improve the performance of 2507 duplex stainless steels by changing the rolling temperature and deformation [20–22]. This method improves the properties without changing the composition, thereby providing potential new approaches for researchers in the field of engineering structural materials research and development; hence, this has become a popular topic in the research of nanomaterials [23,24]. The current methods for micro/nanocrystalline multiphase material preparation mainly include severe plastic deformation, powder metallurgy, and aluminothermic reaction [25–28]. Severe plastic deformation is used mainly to achieve grain refinement by the large plastic strain, and micro-nano crystalline multiphase materials, such as copper-based, aluminum-based, and iron-based materials, have been successfully prepared [28,29]. However, this method is not suitable for processing metals with high yield strength due to the limitation of the strength of the processing equipment and molds [6,30]. Powder metallurgy involves mixing a certain proportion of powders with different particle sizes and then sintering them into a block to obtain materials having different grain sizes. The common processing methods include hot isodiametric extrusion and spark plasma sintering, which have been used to obtain micro-nano structured pure titanium and titanium alloys, pure nickel, nickel alloys, etc. [31–33]. Although this method can obtain precise micro-nano crystalline ratios at an early stage, the alloy is prone to incomplete bonding, impurities, premature failure under tensile stress, or fracture before the start of the yield phenomenon in post-processing. In addition, Wang, et al. found that the variations in the volume fraction, grain size, grain orientation, and grain boundary angle distribution in SAF 2507 duplex stainless steel (DSS) can be optimized to improve the mechanical properties through large- ΔT (large temperature range) thermal cycling [34].

Compared with the above methods, the aluminothermic reaction has the advantages of low cost, low energy consumption, and a simple process, through which larger-sized ingots can be obtained. The main principle of this method is that the oxidation-reduction reactions occur between aluminum and other metal oxides under the action of an ignition agent in the autoclave, and release a large amount of heat so that alloying element powders can be melted into liquid in a short time. The high thermal conductivity of the copper substrate is used to provide a large undercooling degree to prepare bulk material with a grain size mainly distributed at the nanometer and micrometer levels, and further through subsequent heat treatment and rolling to obtain microcrystals ($<1 \mu\text{m}$), ultrafine crystals (500–100 nm), and nanocrystals ($<100 \text{ nm}$) [35,36]. Our research group has prepared large-scale micro-nanocrystalline duplex 304, 316 L stainless steel, hypoeutectoid steel, 1020 steel, 1045 steel, etc., using the aluminothermic reaction [12,35,36]. However, it was found that some elements, such as chromium, evaporated due to the high temperature in the reaction process, and be deposited on the furnace wall, resulting in a larger deviation between the designed and actual compositions. Thus, it is important to control the composition of the alloy prepared by this method.

This work is aimed to prepare micro-nano structure 2507 duplex stainless steels by aluminothermic reaction based on the previous research. In order to make up for the evaporation loss of chromium during the reaction, the excess weight ratios of 50%, 70%, and 100% of chromium were added to the reaction powders for preparing alloys. Further, the 2507 duplex stainless steels with satisfactory composition and structure were rolled

roughly with deformation of 40% at 1000 °C, followed by fine rolling with deformation of 30, 50 and 70%, separately, at 800 °C. Then, the effects of rolling deformation and precipitation on mechanical properties were studied in detail.

2. Experimental

2.1. Material and Processing

In the present study, 2507 duplex stainless steels were prepared by aluminothermic reaction. The specific steps were as follows: first, the design composition of 2507 duplex stainless steels was determined to be 0.02 wt.% carbon, 24.98 wt.% chromium, 7.00 wt.% nickel, 3.99 wt.% molybdenum, 0.28 wt.% nitrogen, 0.50 wt.% manganese, 0.42 wt.% silicon, and 62.81 wt.% iron according to the standard chemical composition (Table 1). A total of 1500 g raw material powders was prepared according to the design composition, in which the ratio of ferric oxide to aluminum as reaction powders (purity \geq 99 wt.%) was determined by Equation (1) [37], and the addition ratios of other elements were 0.01 wt.% carbon, 0.32 wt.% manganese, 0.45 wt.% silicon nitride, 4.45 wt.% nickel, 2.54 wt.% molybdenum, and 15.89 wt.% chromium. The proportion of 15.89 wt.% was defined as the no-excess benchmark of Cr content.

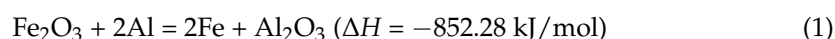


Table 1. Standard chemical composition of 2507 duplex stainless steel [14,38].

Element	C	Cr	Ni	Mo	N	Mn	Si	Fe
wt.%	≤ 0.03	24~26	6~8	3~5	0.24~0.32	≤ 1.2	≤ 0.8	Balance

It was mentioned in the introduction section that chromium is easy to volatilize during the aluminothermic reaction. Therefore, this element was dosed in excess based on the standard addition ratio, and the excessive weight percentages were 50, 70 and 100%. Then, the reactant powders and grinding balls in a ratio of 1:2 were placed into the stainless steel ball mill tanks of the QM-1SP4 planetary ball mill equipment, and were dry ground for 16 h at a speed of 150 r/min. Subsequently, the reactant powder was pressed into several cylindrical billets of Φ 85 mm \times 15 mm and placed in the copper crucible with the surface igniting agents (3 g). Finally, the copper crucible was placed in the reaction vessel before the chamber door was closed, the reaction vessel was filled with 0.5 MPa argon to exhaust the air at room temperature, and the chamber was then heated to 180 °C. Secondly, it was filled with argon at 5.0 MPa and heated again to 260 °C. At this temperature, the igniting agents were ignited, thereby emitting a large amount of heat and then initializing the aluminothermic reaction. The alloys were taken out after the furnace cooled to room temperature. The as-cast steel ingots were 150 mm in diameter and 10 mm in thickness.

The as-cast alloys were cut into 100 \times 50 \times 5 mm³ cuboids by wire cutting and then rolled roughly with deformation of 40% at 1000 °C, followed by fine rolling with deformation of 30, 50 and 70%, separately, at 800 °C (denoted HR-30%, HR-50%, and HR-70%) using a two-roll hot rolling mill to eliminate casting defects and improve the ductility of the alloys. All samples were cooled to room temperature in air after rolling.

2.2. Microstructural and Mechanical Evaluation

The microscopic morphology and composition were analyzed using a JSM-6700F scanning electron microscope and its accessory, as X-ray energy dispersive spectroscope. The analysis of elemental distribution on the surface was carried out by an EPMA-1600 electron probe analyzer. The structure of alloys was characterized by a D8 ADVANCE X-ray diffractometer and a JEM2010 transmission electron microscope having an operating voltage of 200 kV. The transmission electron microscope samples were electrolyzed and thinned with a double-jet electrolyzer, and the electrolyte was 2 vol.% perchloric acid alcohol solution. A VH1102-01-0087 type Blauvis optical hardness tester was used to carry out the hardness test. A WDW-100D universal testing machine was used to carry out the tensile test at a

cross speed of 0.2 mm/min, and the average value was repeated 3 times. The standard deviation was less than 5%. The tensile sample size is shown in Figure 1.

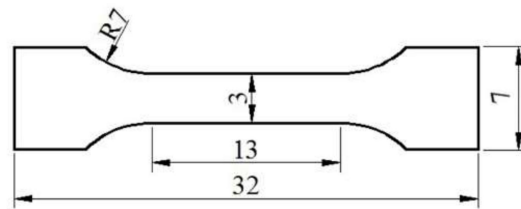


Figure 1. Schematic diagram of tensile sample (unit in mm).

3. Results

3.1. Microstructure

The X-ray diffractometer patterns of the as-cast 2507 duplex stainless steel prepared with different chromium excess ratios show that, when the chromium excess ratios are 50 and 70%, the alloys are composed of γ and α phases, whereas when the excess ratio increases to 100%, it is completely composed of the α phase and free of the duplex structure, which obviously does not meet the requirements of 2507 duplex stainless steels shown in Figure 2. In addition, the change in the X-ray diffraction intensities of γ and α phases with the increase in the chromium excess fraction preliminarily shows that the structure of 2507 duplex stainless steels prepared by the aluminothermic method can be controlled by adjusting the excess fraction of chromium.

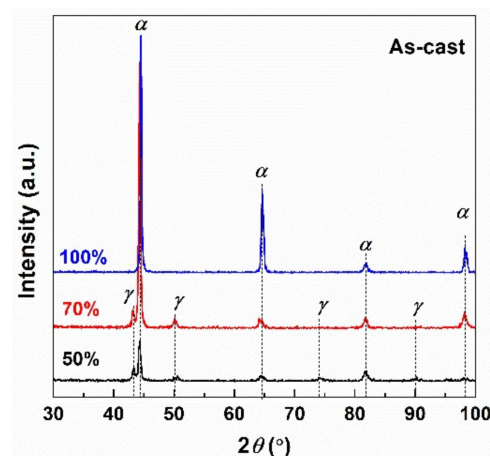


Figure 2. The X-ray diffractometer patterns of 2507 duplex stainless steels prepared with excessive Cr of 50, 70 and 100%.

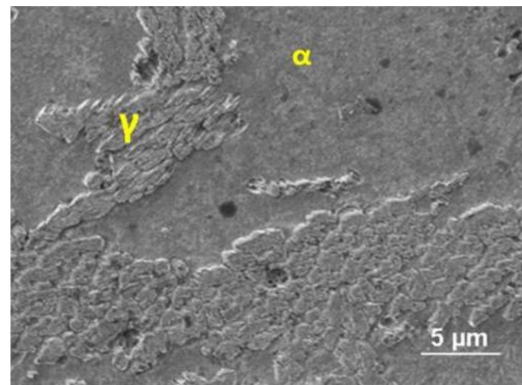
Compared with the standard composition, when the excess ratio of chromium is 70%, the chromium, molybdenum, nickel, and silicon contents in the alloy are basically in line with the composition requirement, and the manganese content is far less than 1.2 wt.%, as shown in Table 2. It should be noted that the difference between the measured and standard content of carbon element is easily attributable to the element's light weight, which caused errors in the detection process. However, when the excess ratios of chromium are 50 and 100%, the chromium content is missing or in surplus, and manganese also cannot be detected.

As shown in Figure 2, the alloy is composed entirely of the α phase as the excess ratio of chromium is 100%, which is mainly due to the fact that chromium is the forming element of the α phase. Furthermore, according to the Schaeffer phase diagram, only the α phase can be formed when the alloy has the present composition. In comparison, when the excess ratio of chromium is 70%, the alloy composition is closest to the design requirements.

Table 2. The EDS results of prepared 2507 duplex stainless steel.

Excess Percentage of Chromium	Composition (wt.%)							
	C	Al	Si	Mo	Cr	Mn	Fe	Ni
50%	1.76	0.36	0.65	4.39	20.87	0.00	65.31	5.99
70%	0.80	1.52	0.81	4.33	24.45	0.12	61.37	6.59
100%	0.08	1.12	0.87	3.67	27.81	0.00	61.10	6.59

According to the scanning electron microscope morphology of the as-cast 2507 duplex stainless steel prepared with excessive chromium of 70%, it can be preliminarily judged that the convex phase is the γ phase and the concave phase is the α phase, as shown in Figure 3 [13]. The volume fraction of γ and α phases are 52 and 48%, respectively, based on the measurement of Image Pro Plus. The volume ratio meets the requirements of 2507 duplex stainless steel for the ratio of these two phases. By combining the EDS and XRD results, it can be concluded that 2507 duplex stainless steels can be obtained when the chromium excess ratio is 70%, which meets both the composition and the structure requirements.

**Figure 3.** SEM image of 2507 duplex stainless steel prepared with excessive Cr of 70%.

The transmission electron microscope bright field image, dark field image, selected area electron diffraction pattern, and nanocrystalline grain size distribution of the as-cast 2507 duplex stainless steel prepared with excessive chromium of 70% are shown in Figure 4. In the bright field image (Figure 4a), the black area indicates the sub-micron or micro-crystal area, and the gray area corresponds to the white bright spot areas in the dark-field image, which are nanocrystals (Figure 4b). The selected area electron diffraction pattern is a series of continuous diffraction rings, indicating that there are many nanocrystals in the selected area. The calibration results reveal that the alloy is mainly composed of γ and α phases, but also contains a small amount of aluminum oxide particles. The volume fraction of nanocrystals is 41% and the average grain size is 34 nm, according to the statistics of ten dark field images produced by Image Pro Plus software; the histogram of the nanocrystalline grain size distribution is shown in Figure 4d. It can be seen that the size of nanocrystals is mainly distributed in the range of 20 to 45 nm.

The X-ray diffractometer patterns of the hot-rolled 2507 duplex stainless steel prepared with excess chromium of 70% show that the alloys are mainly composed of α and γ phases and the intensity of the diffraction peaks do not change with the deformation; Figure 5. However, in HR-70% alloy, there is a small quantity of the sigma (σ) phase in addition to the two main phases due to the eutectoid transformation, i.e., $\alpha \rightarrow \sigma + \gamma_2$; this results from a long residence time, during which the ferrite phase transforms into σ and γ_2 phases. The transformation time is generally 30 min.

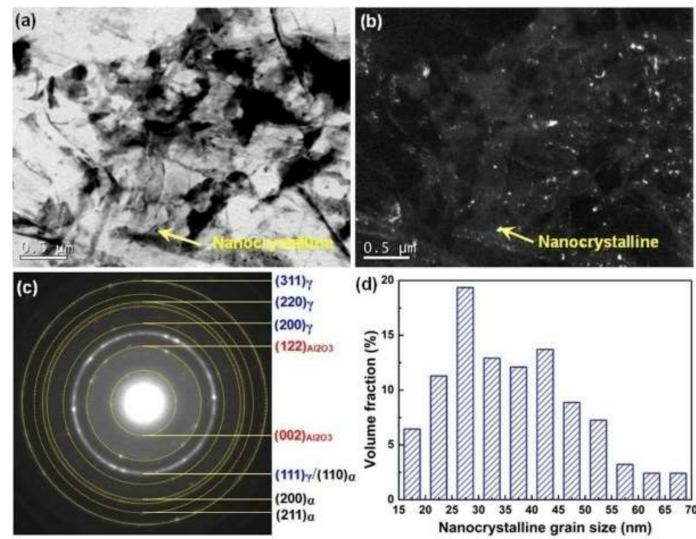


Figure 4. The transmission electron microscope images of as-cast 2507 duplex stainless steels: (a) bright field image; (b) dark field image; (c) selected area electron diffraction pattern; (d) histogram of nanocrystalline grain size distribution.

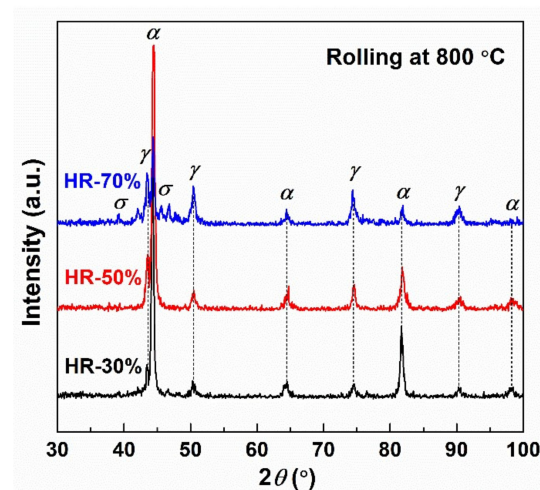


Figure 5. The XRD patterns of hot-rolled 2507 duplex stainless steels.

It can be seen from the electron probe microanalysis backscattered electron images (BEIs) and the corresponding element mappings of 2507 duplex stainless steel with different rolling deformations at 800 °C that the alloys are composed of a gray α phase and a white γ phase; Figure 6. In the HR-30% alloy, the distribution of elements is fundamentally uniform, except for the mapping of aluminum; Figure 6a. As shown in Figure 6b, the segregation of aluminum disappears in the HR-50% alloy. In addition, iron-poor and chromium-rich regions appear in the HR-70% alloy (Figure 6c) and correspond to σ -precipitated regions according to the X-ray diffractometer results.

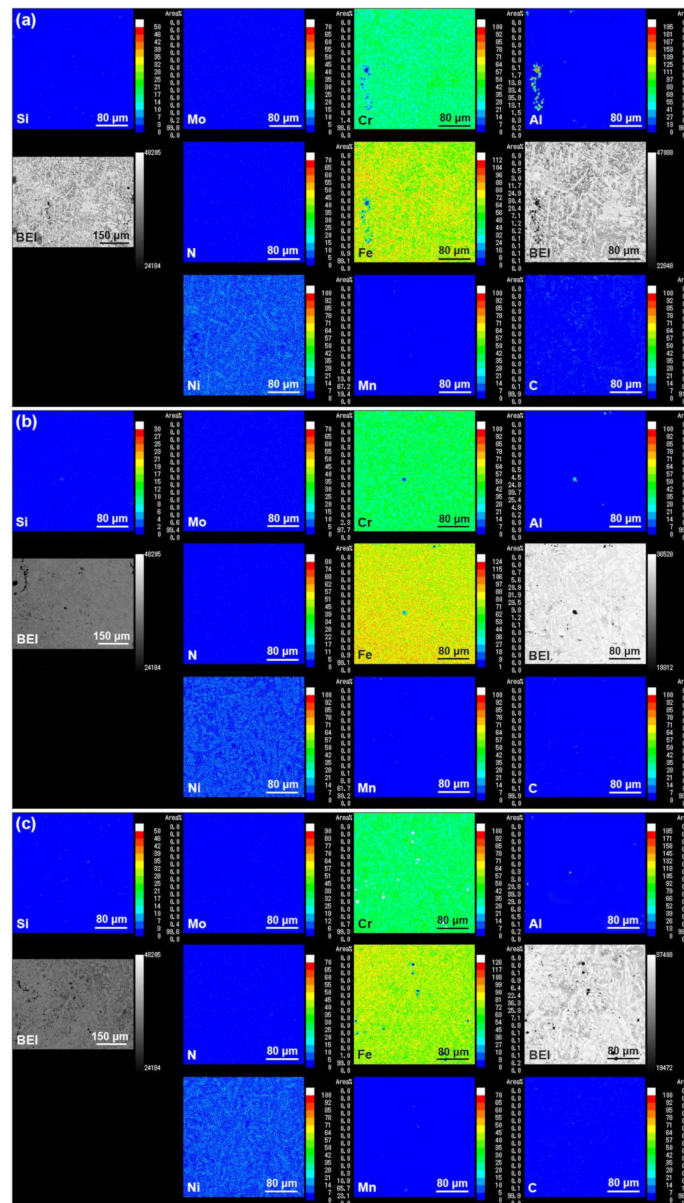


Figure 6. The EPMA backscattered electron images (BEIs) of hot-rolled 2507 duplex stainless steels and their corresponding element mappings: (a) HR-30%; (b) HR-50%; and (c) HR-70%.

3.2. Tensile Tests

The stress–strain curves and the variation trend in the strength and elongation of hot-rolled 2507 duplex stainless steel are shown in Figure 7a,b, respectively. The tensile strength of HR-30%, HR-50%, and HR-70% alloys are 574, 912, and 817 MPa, and the yield strength are 555, 523, and 711 MPa, respectively, indicating that the tensile strength first increases and then decreases with the increase in deformation, but the yield strength shows the opposite trend. With the increase in deformation, the elongations are 8.3, 24.3 and 7.4%, respectively, which shows the same trend with tensile strength. Figure 7c shows that the hardness increases with the increase in rolling deformation, and approaches values of 294, 393, and 418 HV, respectively. However, according to the empirical conversion relationship between hardness and strength, using Equation (2) [39]:

$$\sigma_b = 9.8 \times \left(\frac{2463622}{3031 - \text{HV}} - 801.63 \right) \quad (2)$$

it can be calculated that the tensile strengths of HR-30%, HR-50%, and HR-70% alloys are 965.15, 1296.19, and 1383.76 MPa, which shows a certain gap between the measured and calculated values of tensile strength. The strength converted by hardness is much higher than the actual tensile strength of the material. This is mainly due to the fact that there are trace pores and inclusions in the microstructure of the micro-nano alloy prepared by aluminothermic reaction. After hot-rolling deformation, some pores and other defects in the microstructure disappear, and the grain distribution is much uniform, resulting in the significantly improved mechanical properties of the material (HR-50%). It should also be noted that too many inclusions or precipitates will deteriorate the tensile properties and reduce the tensile strength of materials (HR-70%), but can increase the hardness of the material.

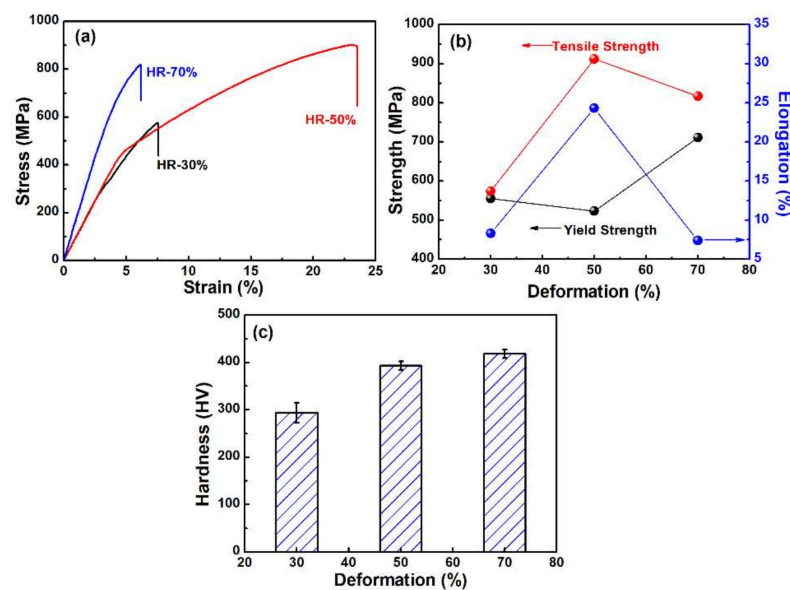


Figure 7. Mechanical properties of hot-rolled 2507 duplex stainless steel: (a) stress–strain curves; (b) strength and elongation; (c) hardness.

The main reason for this finding requires further analysis of their fracture morphologies. The HR-30% alloy has no obvious plastic deformation when viewed macroscopically, the size of the dimples is not uniform, the length and width of the dimples are not consistent, and there are a few cleavage planes, as shown in Figure 8a. It can be seen from the stress–strain curve that this alloy undergoes a ductile–brittle mixed fracture. The HR-50% alloy (Figure 8b) has obvious necking deformation in the macroscopic view. Dimples and tearing surfaces of different sizes can be clearly observed, and the fracture surface is not flat, indicating that the alloy undergoes a ductile fracture. However, in the HR-70% alloy (Figure 8c), a large number of dimples with inconsistent sizes and shallow depths can be observed. In comparison, this alloy does not show the best performance, which is mainly due to the appearance of σ , which reduced the toughness and the elongation. According to the comprehensive assessment of the properties and fracture morphologies, the HR-50% alloy achieves the best performance [40,41].

The chemical reaction heat released by the reduction of certain metal oxides with aluminum can be used to complete the oxide reduction reaction and obtain separated alloys and slags without the need for external heat supplementation. The aluminothermic reaction process is mainly used to produce ferroalloys and intermediate alloys containing high melting point metals and refractory elements. However, due to the fast reaction, it is difficult to achieve equilibrium conditions. As a result, there are more inclusions and precipitation in the subsequent hot-rolling process of alloy and stainless steel, which affects the mechanical properties of materials.

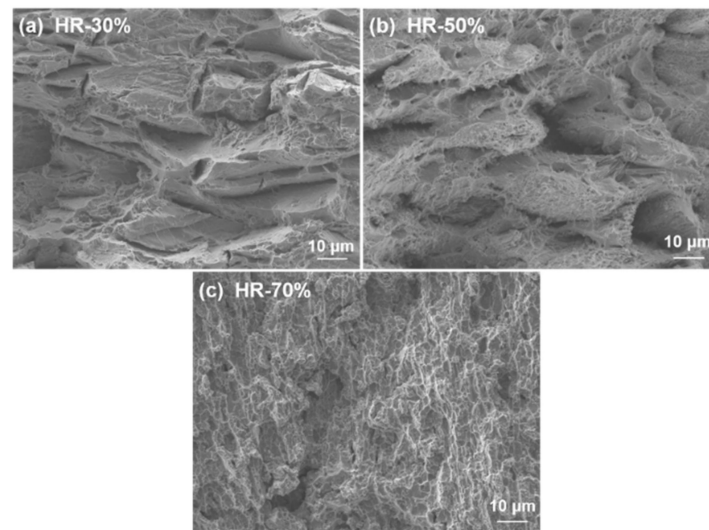


Figure 8. Fracture morphologies of hot-rolled 2507 duplex stainless steels: (a) HR-30%; (b) HR-50%; and (c) HR-70%.

4. Discussion

According to the alloy composition and structure analysis, it can be seen that the micro-nano structure 2507 duplex stainless steels having compositions close to the design ratio can be successfully prepared by aluminothermic reaction. This is mainly because this preparation method can release a lot of heat; thus, all alloy elements can be fully melted in a short period. Due to the high temperature, the non-metallic elements in the alloy evaporate, melt, and float, thereby effectively purifying the melt. However, the evaporation of these nonmetals and chromium also causes the formation of pores during solidification. When solid crystal nuclei are formed in the super-cooled metallic liquids, both homogeneous and heterogeneous nucleation may occur simultaneously. Apparently, the metallographic results show that there are some small pores in the structure, and the transmission electron microscope analysis indicates that the distribution of nanocrystals is not very uniform. Therefore, the as-cast micro-nano structured alloy shows poor plasticity and is not conducive to subsequent processing due to the presence of nanocrystals and a small number of pores. Thus, it is necessary to further improve the microstructure of the alloy and adjust the nanocrystalline distribution.

In the rolling process of 2507 duplex stainless steel, the grain refinement is beneficial to improving the strength of the material with increasing rolling deformation. As nanocrystals will grow into submicron crystals when rolled at high temperature, their distribution is collectively determined by the rolling temperature and deformation. The stress distribution and plastic strain at the initial stage of rolling deformation are almost accommodated by ferrite, and then the load transfers from ferrite to austenite with a higher strain. In the softening mechanism of the ferrite phase in the rolling process, the dynamic recovery and continuous dynamic crystallization exist simultaneously, whereas the austenite phase comprises discontinuous dynamic recrystallization [38]. In addition, the grain breakage is more obvious with larger rolling deformation. This results in increases in the grain and phase boundaries, which delay the crack propagation and fracturing of the alloy. The deformation mechanism of micro-nano structured metals is still dominated by dislocation slip, and cracks grow along the boundaries of nanocrystals, so that the final fracture is caused by the strength mismatch between microcrystalline and nanocrystalline materials.

In the present work, there was a transformation from the α phase to γ phase with the increase in the rolling deformation at 800 °C for the 2507 duplex stainless steel prepared with excessive chromium of 70%. The hardness increased monotonically with the amount of deformation. However, the tensile strength and plasticity decreased significantly due to the eutectoid transformation in the HR-70% alloy, namely $\alpha \rightarrow \sigma + \gamma_2$. The σ phase is a hard

brittle intermetallic compound rich in chromium and molybdenum, which greatly reduces the ductility and toughness of duplex stainless steel [42,43]. Thus, with the continuous precipitation of the σ phase, the strength increases and the elongation reduces gradually.

5. Conclusions

In summary, 2507 duplex stainless steels having a micro-nano structure were prepared by a one-step method with the aluminothermic reaction. The comparative analysis shows that, for a chromium excess of 70%, a satisfactory composition and organization structure were obtained for the 2507 duplex stainless steel prepared by this method. In the as-cast steel, the volume ratio of the γ to the α phase was basically 1:1, the volume fraction of nanocrystals was 41%, and the average grain size was 34 nm. Further, the steels were rolled roughly with deformation of 40% at 1000 °C, followed by fine rolling with deformation of 30, 50 and 70%, separately, at 800 °C. The HR-30% and HR-50% alloys were also composed of γ and α phases, but, in the HR-70% alloy, the eutectoid reaction occurred to form the σ phase. The hardness of the alloy increased with the increase in the rolling deformation, and was 294, 393, and 418 HV, respectively. The tensile strength and plasticity first increased and then decreased with the amount of deformation; that is, when the deformation was 50%, the rolled alloy achieved the best performance and showed the characteristics of a ductile fracture. The optimized tensile strength, yield strength, and elongation were 912 MPa, 523 MPa, and 24.3%, respectively. Obviously, steel materials with excellent comprehensive properties can be obtained by adjusting the microstructure through the aluminothermic reaction and following the deformation process, which provides theoretical and experimental support for the development and popularization of such engineering structural materials.

Author Contributions: Conceptualization, M.Z. and P.L.; methodology, F.Z. and M.Z.; formal analysis, F.Z. and Y.Z.; investigation, K.W. and S.X.; data curation, K.W., X.L. and H.Z.; writing—original draft preparation, M.Z. and F.Z.; writing—review and editing, F.Z. and Y.Z.; project administration, P.L.; funding acquisition, P.L. and F.Z. All authors have read and agreed to the published version of the manuscript.

Funding: This research was funded by the University Innovation Fund of Gansu Province in 2020 (Grant no. 2020A-030), the Tamarisk Outstanding Young Talents Program of Lanzhou University of Technology, and the Open Project Fund of Gansu Key Laboratory of Solar Power System Engineering Project (Grant no. 2022SPKL04).

Conflicts of Interest: The authors declare no conflict of interest.

References

1. Feng, H.; Zhou, X.Y.; Liu, H.; Song, Z.G. Development and trend of hyper duplex stainless steels. *J. Iron Steel Res.* **2015**, *27*, 1–5.
2. Fan, Y.; Liu, T.; Xin, L.; Han, Y.; Lu, Y.; Shoji, T. Thermal aging behaviors of duplex stainless steels used in nuclear power plant: A review. *J. Nucl. Mater.* **2021**, *544*, 152693–152706. [[CrossRef](#)]
3. Li, J.; Li, G.; Liang, W.; Han, P.; Wang, H. Effect of Aging on Precipitation Behavior and Pitting Corrosion Resistance of SAF2906 Super Duplex Stainless Steel. *J. Mater. Eng. Perform.* **2017**, *26*, 4533–4543. [[CrossRef](#)]
4. George, P.; Wins, K.L.D.; Dhas, D.E.J.; George, P. Machinability, weldability and surface treatment studies of SDSS 2507 material—A review. *Mater. Today Proc.* **2021**, *46*, 7682–7687. [[CrossRef](#)]
5. Du, J.-K.; Chao, C.-Y.; Wei, L.-L.; Wang, C.-H.; Chen, J.-H.; Chen, K.-K.; Huang, R.-B. Effects of Ag-Rich Nano-Precipitates on the Antibacterial Properties of 2205 Duplex Stainless Steel. *Metals* **2021**, *11*, 23. [[CrossRef](#)]
6. Chen, M.; Liu, H.; Wang, L.; Xu, Z.; Ji, V.; Jiang, C. Residual stress and microstructure evolutions of SAF 2507 duplex stainless steel after shot peening. *Appl. Surf. Sci.* **2018**, *459*, 155–163. [[CrossRef](#)]
7. Li, J.; Ma, Z.; Xiao, X.; Zhao, J.; Jiang, L. On the behavior of nitrogen in a low-Ni high-Mn super duplex stainless steel. *Mater. Des.* **2011**, *32*, 2199–2205. [[CrossRef](#)]
8. Torres, C.; Johnsen, R.; Iannuzzi, M. Crevice corrosion of solution annealed 25Cr duplex stainless steels: Effect of W on critical temperatures. *Corros. Sci.* **2021**, *178*, 109053–109066. [[CrossRef](#)]
9. Li, J.; Zhang, Z.; Chen, H.; Xiao, X.; Zhao, J.; Jiang, L. New Economical 19Cr Duplex Stainless Steels. *Met. Mater. Trans. A* **2012**, *43*, 428–436. [[CrossRef](#)]
10. Llorca-Isern, N.; López-Luque, H.; López-Jiménez, I.; Biezma, M.V. Identification of sigma and chi phases in duplex stainless steels. *Mater. Charact.* **2016**, *112*, 20–29. [[CrossRef](#)]

11. He, L. Microstructure Evolution and Corrosion Behavior of Duplex Stainless Steel During Isothermal Aged at 650 °C. *Int. J. Electrochem. Sci.* **2016**, *11*, 8046–8056. [[CrossRef](#)]
12. Li, Z.; Wei, F.; La, P.; Wang, H.; Wei, Y. Enhancing Ductility of 1045 Nanoeutectic Steel Prepared by Aluminothermic Reaction through Annealing at 873K. *Adv. Mater. Sci. Eng.* **2017**, *2017*, 5392073. [[CrossRef](#)]
13. Mao, Y.; Zheng, Y.; Shi, Y.; Zhu, M.; Saitejin; Liu, S.; Lin, X.; La, P. Effect of rolling deformation on microstructure and mechanical properties of 2205 duplex stainless steel with micro-nano structure. *Mod. Phys. Lett. B* **2020**, *34*, 2050269–2050280. [[CrossRef](#)]
14. Zhang, W.; Zou, D.N.; Fan, G.W.; Li, J. Influence of Aging Time on Sigma Phase Precipitation in SAF2507 Super-Duplex Stainless Steel. *Mater. Sci. Forum* **2009**, *620–622*, 355–358. [[CrossRef](#)]
15. Wang, Y.; Sun, H.; Li, J.; Li, D.; Li, N. Pitting Corrosion of Thermally Aged Duplex Stainless Steels at Different Temperature for Long Time. *Mater. Res.* **2019**, *22*, e20180663. [[CrossRef](#)]
16. Lin, P.-C.; Tsai, Y.-T.; Gan, N.-H.; Yang, J.-R.; Wang, S.-H.; Chang, H.-Y.; Lin, T.-R.; Chiu, P.-K. Characteristics of Flakes Stacked Cr₂N with Many Domains in Super Duplex Stainless Steel. *Crystals* **2020**, *10*, 965. [[CrossRef](#)]
17. Mészáros, I.; Bögre, B.; Szabó, P.J. Magnetic and Thermoelectric Detection of Sigma Phase in 2507 Duplex Stainless Steel. *Crystals* **2022**, *12*, 527. [[CrossRef](#)]
18. Berecz, T.; Fazikas, É.; Fábrián, E.R.; Jenei, P.; Marióti, J.E. Investigation of Thermally Induced Deterioration Processes in Cold Worked SAF 2507 Type Duplex Stainless Steel by DTA. *Crystals* **2020**, *10*, 937. [[CrossRef](#)]
19. Chen, M.; Liu, H.; Wang, L.; Wang, C.; Zhu, K.; Xu, Z.; Jiang, C.; Ji, V. Evaluation of the residual stress and microstructure character in SAF 2507 duplex stainless steel after multiple shot peening process. *Surf. Coat. Technol.* **2018**, *344*, 132–140. [[CrossRef](#)]
20. Zheng, Z.; Liu, J.; Gao, Y. Achieving high strength and high ductility in 304 stainless steel through bi-modal microstructure prepared by post-ECAP annealing. *Mater. Sci. Eng. A* **2017**, *680*, 426–432. [[CrossRef](#)]
21. Kb, A.; Jm, B.; Mf, B.; Kec, D.; Zhc, D. Effect of high-pressure torsion on grain refinement, strength enhancement and uniform ductility of EZ magnesium alloy-ScienceDirect. *Mater. Lett.* **2018**, *212*, 323–326.
22. Zhizhong, S.; Henry, H.; Xiang, C.; Qigui, W.; Wenyong, Y. Gating system design for a magnesium alloy casting. *J. Mater. Sci. Technol.* **2008**, *24*, 93–95.
23. Wang, H.-D.; La, P.-Q.; Shi, T.; Wei, Y.-P.; Lu, X.-F. Research status and development trend of bulk nano/micro-crystalline composite metallic materials. *J. Mater. Eng.* **2013**, *3*, 92–96.
24. Świeboda, C.; Leszczyński, J. Influence of production technology on magnetic properties of nanocrystalline stacked and block magnetic cores. *Prz. Elektrotechniczny* **2016**, *92*, 281–285. [[CrossRef](#)]
25. Cheng, W.; Tian, L.; Ma, S.; Bai, Y.; Wang, H. Influence of Equal Channel Angular Pressing Passes on the Microstructures and Tensile Properties of Mg-8Sn-6Zn-2Al Alloy. *Materials* **2017**, *10*, 708. [[CrossRef](#)] [[PubMed](#)]
26. Mao, X.; Kang, S.H.; Kim, T.K.; Kim, S.C.; Oh, K.H.; Jang, J. Microstructure and Mechanical Properties of Ultrafine-Grained Austenitic Oxide Dispersion Strengthened Steel. *Met. Mater. Trans. A* **2016**, *47*, 5334–5343. [[CrossRef](#)]
27. Guo, X.; Yang, G.; Weng, G. The saturation state of strength and ductility of bimodal nanostructured metals. *Mater. Lett.* **2016**, *175*, 131–134. [[CrossRef](#)]
28. Korn, M.; Lapovok, R.; Bohner, A.; Hoppel, H.W.; Mughrabi, H. Bimodal grain size distributions in UFG materials produced by SPD—Their evolution and effect on the fatigue and monotonic strength properties. *Met. Mater.* **2011**, *49*, 51–63. [[CrossRef](#)]
29. Azushima, A.; Kopp, R.; Korhonen, A.; Yang, D.Y.; Micari, F.; Lahoti, G.D.; Groche, P.; Yanagimoto, J.; Tsuji, N.; Surochowski, A.; et al. Severe plastic deformation processes for metals. *CIRP Ann.* **2008**, *57*, 716–735. [[CrossRef](#)]
30. Segal, V. Review: Modes and Processes of Severe Plastic Deformation (SPD). *Materials* **2018**, *11*, 1175. [[CrossRef](#)]
31. Fang, Z.Z.; Paramore, J.D.; Sun, P.; Chandran, K.R.; Zhang, Y.; Xia, Y.; Cao, F.; Koopman, M.; Free, M. Powder metallurgy of titanium-past, present, and future. *Int. Mater. Rev.* **2018**, *63*, 407–459. [[CrossRef](#)]
32. Mahdih, S.O.; Hamed, A.; Sina, S.; Mozhgan, S. Significant Corrosion Resistance in an Ultrafine-Grained Al6063 Alloy with a Bimodal Grain-Size Distribution through a Self-Anodic Protection Mechanism. *Metals* **2016**, *6*, 307.
33. Zhao, Y.; Topping, T.; Bingert, J.F.; Thornton, J.J.; Dangelewicz, A.M.; Li, Y.; Liu, W.; Zhu, Y.; Zhou, Y.; Lavernia, E.J. High Tensile Ductility and Strength in Bulk Nanostructured Nickel. *Adv. Mater.* **2008**, *20*, 3028–3033. [[CrossRef](#)]
34. Yu, P.-J.; Chen, S.-C.; Yen, H.-W.; Chang, H.-Y.; Yang, J.-R.; Wang, S.-H.; Chiu, P.-K.; Lin, T.-R. Large Delta T Thermal Cycling Induced Stress Accelerates Equilibrium and Transformation in Super DSS. *Crystals* **2020**, *10*, 962. [[CrossRef](#)]
35. Wei, F.; La, P.; Ma, F.; Donic, T.; Wang, H. Enhanced intergranular corrosion resistance and tensile strength in 304 stainless steel with dispersed nanocrystallines in microcrystalline austenite. *J. Mater. Res.* **2016**, *31*, 1691–1701. [[CrossRef](#)]
36. La, P.; Guo, X.; Wang, H.; Shi, T.; Zhen, X.; Wei, F.; Lu, X. Effect of annealing temperature on the microstructure and tensile properties of a bimodal nano/micro grained 1020 carbon steel prepared by aluminothermic reaction casting. *Met. Mater. Int.* **2016**, *22*, 236–242. [[CrossRef](#)]
37. Aghili, S.; Enayati, M.; Karimzadeh, F. Synthesis of (Fe, Cr)₃Al-Al₂O₃ nanocomposite through mechanochemical combustion reaction induced by ball milling of Cr, Al and Fe₂O₃ powders. *Adv. Powder Technol.* **2014**, *25*, 408–414. [[CrossRef](#)]
38. Mishra, M.K.; Balasundar, I.; Rao, A.G.; Kashyap, B.P.; Prabhu, N. On the High Temperature Deformation Behaviour of 2507 Super Duplex Stainless Steel. *J. Mater. Eng. Perform.* **2017**, *26*, 802–812. [[CrossRef](#)]
39. Qingshan, W. Empirical formula for strength-hardness conversion of ferrous metals. *Phys. Test. Chem. Anal. Part A Phys. Test.* **1995**, *31*, 39–40.

40. Macek, W.; Pejkowski, Ł.; Branco, R.; Nejad, R.M.; Žak, K. Fatigue fracture surface metrology of thin-walled tubular austenitic steel specimens after asynchronous loadings. *Eng. Fail. Anal.* **2022**, *138*, 106354–106371. [[CrossRef](#)]
41. Azevedo, C.R.d.F.; Marques, E. Three-dimensional analysis of fracture, corrosion and wear surfaces. *Eng. Fail. Anal.* **2010**, *17*, 286–300. [[CrossRef](#)]
42. Han, Y.; Zou, D.N.; Zhang, W.; Huang, R. Sigma Phase Precipitation of Duplex Stainless Steel and its Effect on Corrosion Resistance. *Mater. Sci. Forum* **2009**, *620*, 391–394. [[CrossRef](#)]
43. Wang, Y.Q.; Han, J.; Wu, H.C.; Yang, B.; Wang, X.T. Effect of sigma phase precipitation on the mechanical and wear properties of Z3CN20.09M cast duplex stainless steel. *Nucl. Eng. Des.* **2013**, *259*, 1–7. [[CrossRef](#)]